View metadata, citation and similar papers at core.ac.uk
brought to you by CORE
provided by University of Liverpool Repository

Band Line-up of High-k Oxides on GaN

Ivona Z. Mitrovic[a], Partha Das[b], Leanne A.H. Jones[c], James T. Gibbon[c],
Vinod R. Dhanak[c], Rajat Mahapatra[b], Teresa Partida-Manzanera[d], Joseph W. Roberts[d],
Richard Potter[d], Paul R. Chalker[d], Sung-Jin Cho[e], Iain G. Thayne[e]

[a]Dept. of Electrical Engineering & Electronics, University of Liverpool, L69 3GJ, UK
[b]Dept. of Electronics and Communication Engineering, NIT Durgapur, 713209, India
[c]Department of Physics and SIRE, University of Liverpool, L69 7ZF, UK
[d]School of Engineering, University of Liverpool, L69 3GH, UK
[e]School of Engineering, University of Glasgow, Glasgow G12 8LT, UK

We present comprehensive experimental work on $Ti_xAl_{1-x}O_y$ (with x = 9%, 16%, 25%, 36%, 100%) and $Ga_xAl_{1-x}O_y$ (x = 5%, 20%, 80% and 95%) fabricated using atomic layer deposition with the aim of achieving favorable band alignment with GaN for device applications. The permittivity, k, has been found to be enhanced from ~10 for 9% Ti to 76 for TiO_2, but brings unfavorable band line-up and a small conduction band offset (< 0.1 eV) with GaN for all Ti% studied. On the other hand, $Ga_xAl_{1-x}O_y$ (x = 5%, 20%) films show substantial increase of the band gap from 4.5 eV for Ga_2O_3 to 5.5 eV for x = 5% Ga and 6.0 eV for x = 20% Ga in mixed oxides and a strong suppression of leakage current in associated metal insulator semiconductor (MIS) capacitors.

Introduction

GaN high electron mobility transistors (HEMTs) have been commercially available for over 10 years, however gate leakage limits their performance. The HEMT has the advantages of offering simple associated circuit design and fail-safe operation. Currently the GaN based MIS-HEMT device is seen to demonstrate superior performance in power electronics applications over the Schottky gate counterpart, due to its inherently lower gate leakage current, together with the ability to provide larger forward gate voltage swing and an improved gate-drain breakdown voltage (1,2). High band gap gate dielectric materials, such as Al_2O_3 (3), are preferable as they can provide higher tunnelling barriers for electrons and holes resulting in lower gate leakage current. On the other hand, high dielectric constant (high-k) material is also necessary for improved electrostatic control over the channel and improved on-current, which in-turn results in higher transconductance (4). The quality of the gate dielectric and the oxide/GaN interface plays a central role in device performance due to potential problems arising from fixed oxide charge, border and interface traps (3). The leakage current issue has been mitigated using Al_2O_3 (3,5), SiO_2 (6) and Si_3N_4 (7), but comes at a cost of device transconductance degradation and undesirable threshold voltage shifts. A number of high-k dielectrics such as HfO_2 (4,8), ZrO_2 (9,10), Ta_2O_5 (11), $LaLuO_3$ (12) and TiO_2 (13,14) have been investigated.

In this paper, engineered high-k oxide approach will be presented with (i) Al_2O_3 being doped with Ti to boost oxide permittivity value with the aim of preserving band offsets, as

well as (ii) Ga_2O_3 doped with Al to increase band gap and maintain good interface quality with GaN. X-ray photoelectron spectroscopy (XPS), inverse photoemission spectroscopy (IPES) and variable angle spectroscopic ellipsometry (VASE) were used to determine the band alignment and interfacial properties of deposited high-k oxide/GaN stacks. TiO_2 is very attractive due to having reported k of 20-86 (15,16) but has a small band gap of 3.4 eV for amorphous and 3.26 eV for anatase TiO_2 (17) and a low crystallization temperature of 370ºC (18). Al_2O_3 on the other hand has a sufficient band offset of 1.8-2 eV with AlGaN but suffers from a low dielectric constant of ~7-9 depending on the growth method (19). The previous studies of Al_2O_3/TiO_2 nanolaminates (20,21) show favorable properties, in particular the optimum between the rather high-k (~30) and low leakage current has been observed for 30% Ti (22). No band offset study has been reported for $Al_{1-x}Ti_xO_y$/GaN. Full band alignment study of $Al_{1-x}Ti_xO_y$/GaN fabricated by atomic layer deposition (ALD) on GaN will be presented for the range of Ti content (x) of up to 40%.

Furthermore, a trivalent Ga_2O_3 is a promising oxide due to its band gap of 4.4 - 4.9 eV (23,24) and a moderate permittivity of 10-14.2 (25). Thermally oxidized Ga_2O_3 has shown valence band offset (VBO) of 1.4 eV to GaN (26). A drawback of thermal oxidation is a growth of non-stoichiometric oxide at GaN interface reported to be as $Ga_{(x+2)}N_{3x}O_{(3-3x)}$ (27). In contrast, ALD has been shown to produce Ga_2O_3 with no interfacial layer with GaN and with low density of interface states of 3.62×10^{11} $cm^{-2}eV^{-1}$ (23). Despite the good interface with GaN, the issue with using Ga_2O_3 is a small conduction band offset (CBO < 1 eV) leading to high leakage current. Al_2O_3 has larger band gap (6.4-6.9 eV) and good interface properties to GaN, however current Al_2O_3/GaN/AlGaN MIS-HEMTs suffer from threshold voltage instability and current collapse (5,28,29). The objective of this work was to explore Al doping of Ga_2O_3 by ALD with the aim of maintaining sufficiently high band offsets with GaN while preserving good quality interface.

Experimental Details

ALD was performed using a Cambridge Nanotech Savannah 100 reactor. The TiAlO films of (nominal) 3 nm and 20 nm were deposited using trimethylaluminum (TMA) and titanium isopropoxide (TTIP) as Al and Ti precursors and H_2O as the oxygen-containing co-reactant. The TMA, TTIP and H_2O were transported with 10 sccm zero-grade nitrogen. The TTIP was heated to 90˚C with the substrate held at 200˚C. The number of ALD cycles was used to control the thickness of the films. 1 TMA cycle consisted of a 20 ms TMA dose/ 2 s purge/ 20 ms H_2O dose/2 s purge whereas 1 TTIP cycle consisted of a 1 s TTIP dose/ 10 second purge/ 20 ms H_2O dose/ 2 s purge. Delta doping was utilised to achieve Ti-doped Al_2O_3 films, where TMA cycles were interspersed periodically within the TTIP cycles. The 2 µm n-GaN/Si substrates were cleaned for 5 min in acetone, 5 min in isopropyl alcohol and 2 min in deionized water (all steps sonicated) followed by drying with N_2. The reference samples of TiAlO films on n-Si(100) were fabricated simultaneously in the ALD chamber to determine thickness and optical properties of the films using VASE. Al top electrodes of different diameters (0.25-2 mm) were deposited on 20 nm TiAlO/GaN by thermal evaporation through a shadow mask to process MIS capacitors for electrical characterization, including capacitance voltage (CV) and current voltage (IV).

In case of Ga_2O_3 and $Ga_xAl_{1-x}O_y$ films, 1 ALD cycle of Ga_2O_3 consisted of the substrate (3 nm GaN/20 nm $Al_{0.2}Ga_{0.8}N$/GaN/accumulation layer/seed layer/Si(111)) being held at

250°C, 0.1 s of triethylgallium, 5 s purge to remove any unreacted precursor or by products, 30 s 20 sscm O_2 flow stabilization, 5 s 300 W O_2 plasma and a final 5 s purge. For the $Ga_xAl_{1-x}O_y$ films, different numbers of Al_2O_3 and Ga_2O_3 ALD cycles were used to vary doping from 5% to 95% Al. The Al_2O_3 ALD cycle was a 0.03 s of TMA precursor followed by a 3 s purge, 0.02 s of H_2O and a final 3 s purge. The substrates have undergone the same ex-situ chemical cleaning described above. The CV and IV measurements were performed on MIS capacitors, using a ring capacitor layout, with ~200 μm central diameter and a 20 μm gap to the outer ring. The metallization for the outer ring was Ti/Al/Ni/Au (20/120/20/45 nm) followed by rapid thermal anneal (RTA) in N_2 for 30 s at 850°C. The top contact was Ni/Au (20/200 nm). Some MIS devices underwent the forming gas anneal (10% H_2/90% N_2) (FGA) at 430°C for 30 minutes.

Spectroscopic ellipsometry measurements were conducted using a J.A. Woollam VASE ellipsometer with a spectral range of 0.7-5.2 eV at 60-75˚ in 5˚ steps. Photoelectron spectroscopy (PES) measurements for bulk (20 nm) and interfacial (3 nm) oxide/GaN samples were performed in a standard ultra-high vacuum (UHV) chamber operating at a base pressure of $2x10^{-10}$ mbar. Core level (CL) structure and the occupied density of states in the valence band (VB) were probed by XPS using a SPECS monochromatic Al Kα X-ray source (hν = 1486.6 eV) operating at 250 W, and a PSP Vacuum Technology electron energy analyzer. The spectrometer was operated with an overall resolution of 0.5 eV measured by the full width at half maximum (FWHM) of Ag $3d_{5/2}$ CL. Charging of the samples was corrected by setting the C 1s peak (arising from adventitious carbon species) to 284.80 eV. The unoccupied density of states in the conduction band (CB) was measured by IPES using a PSP Vacuum Technology BaO cathode dispenser electron source and an isochromat NaCl photon detector. The IPES detector operates at a nominal resolution of 0.8 eV. The energy scale was calibrated using the Fermi energy of a clean polycrystalline silver foil. A Shirley-type background was used for the fitting of all XPS CL spectra (30). The uncertainty of ±0.05 eV is stated for fitting XPS CLs by Voigt functions. The error bar (± 0.25 eV) in determining VBO in this paper is due to the valence band maximum (VBM) estimation using the linear interpolation method (31).

ALD $Ti_xAl_{1-x}O_y$ films on GaN

Band alignment of $Ti_xAl_{1-x}O_y$ on GaN

Band gap study. The measured and fitted SE (Ψ, Δ) parameters vs. photon energy (E) are shown in Fig. 1. Since Al_2O_3 is a transparent material, Cauchy model (32) was used for the SE data fitting, whereas for TiO_2 a Cody-Lorentz general oscillator model (33) was used due to its UV-absorbing nature. The SE data for Ti-doped Al_2O_3 films were fitted using the Bruggeman Effective Medium Approximation (EMA) model, as the latter allows for a self-consistent choice of the host material. Two materials, Al_2O_3 and TiO_2 as material 1 and material 2 respectively, were placed into the EMA model. The 'EMA % (Mat 2)' parameter was a variable fit parameter representing the percentage of material 2 in the composite. The mean squared error (MSE) between the experimental and theoretical (fitted) (ψ, Δ) versus E curves was in all cases below 5, consistent with a good quality fit of the data shown in Fig. 1. From the ellipsometry modeling, the Ti content in the films (x) was found to be 9% (2:1=Al:Ti cycles), 16% (1:1 = Al:Ti cycles), 25% (1:2 = Al:Ti cycles) and 36% (1:4 = Al:Ti cycles) in agreement with values calculated from the ALD growth

rates and number of cycles used for Al_2O_3 and TiO_2 to fabricate mixed oxide films (Fig. 2). It has been observed that the growth rate decreases for films with increased Ti %.

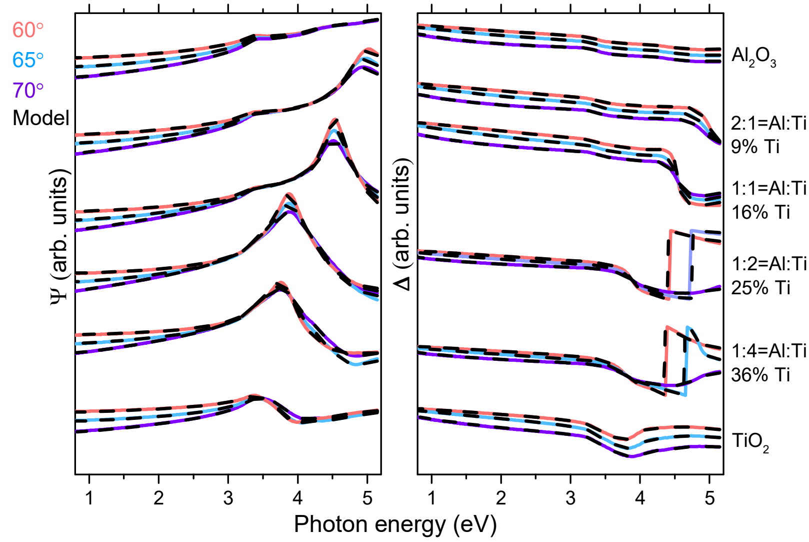

Figure 1. Measured and fitted spectroscopic ellipsometric (Ψ, Δ) parameters vs. photon energy for ALD $Ti_xAl_{1-x}O_y$ (x< 40%) films with Al_2O_3 and TiO_2 as reference samples.

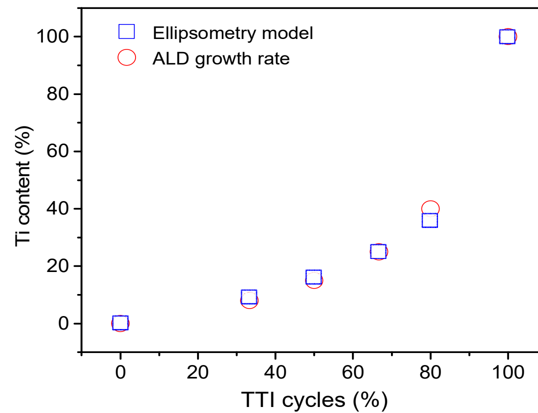

Figure 2. The derived Ti content (x) for the ALD mixed oxide films ($Ti_xAl_{1-x}O_y$) from ellipsometry data and theoretically predicted from the ALD growth rate.

The thickness of the films (summarized in Table I), refractive index (n) and extinction coefficient (κ) were extracted from the SE modelling; the absorption coefficient (α) can be found from the extinction coefficient as

$$\alpha = \frac{4\pi\kappa(E)E}{hc} \qquad [1]$$

where h is the Planck's constant, c is the speed of light, and E is the photon energy. The plots of α vs. E for $Ti_xAl_{1-x}O_y$ and TiO_2 are shown in Fig. 3(a). The linear extrapolation of segments on the curves in the non-absorbing regions in Fig. 3(a) gives the band gap (E_g) values (± 0.1 eV) of TiO_2 of 3.65 eV and of $Ti_xAl_{1-x}O_y$ films varying from 4.28 eV to 3.88 eV as Ti doping increased from 9% to 36% respectively. The latter are in agreement with

band gap data of 4.0 eV for 20% Ti and 3.8 eV for 30-40% Ti extracted from reflection electron energy loss spectroscopy (REELS) (22). The reported values for the optical band gap of TiO_2 have been found to be dependent on the crystallinity of the film and vary from 3.2 eV (22), 3.37 eV (34) to 3.7 eV (35). The band gap of Al_2O_3 was extracted from XPS O 1s energy loss spectrum (ELS) (36) shown in Fig. 3(b) and found to be 6.48 ± 0. 25 eV, in close agreement with optical band gap value (6.43 eV) extracted by vacuum ultra-violet (VUV)-VASE using α-method (37).

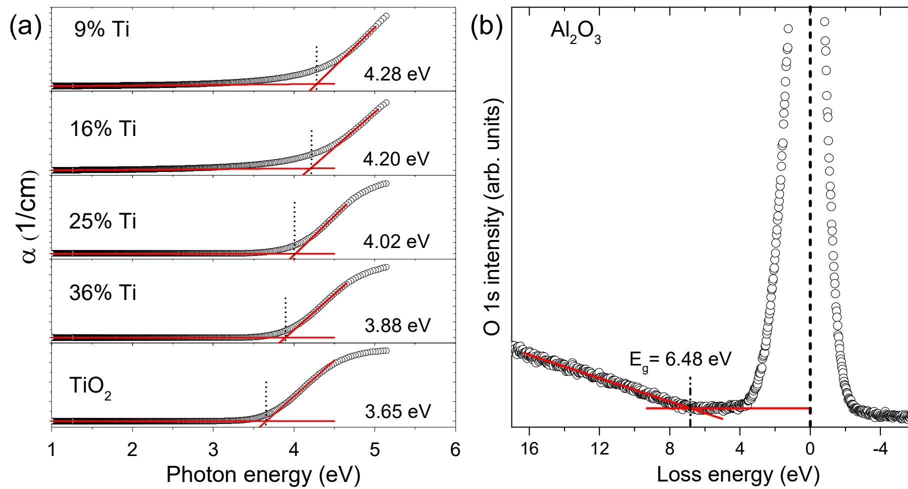

Figure 3. (a) α vs. photon energy plots for $Ti_xAl_{1-x}O_y$ films, with x varying from 9% to 100% (TiO_2); (b) XPS O 1s ELS spectrum depicting extraction of the band gap for Al_2O_3.

Band offsets study. The Al 2p, Ti 2p and O 1s XPS CLs measured for $Ti_xAl_{1-x}O_y$/GaN stacks are shown in Figs. 4(a), (b) and (c) respectively. It can be seen that the Al 2p CL shifts to the lower binding energy (BE) for up to 0.63 eV (Fig. 4(a)) while the Ti $2p_{3/2}$ BE increases by 0.13 eV (Fig. 4(b)) with the increase of Ti % in the $Ti_xAl_{1-x}O_y$ films. Similar trend has been reported when TiO_2 and Al_2O_3 are mixed (38,39) and is due to differing electronegativities of Al (1.61) and Ti (1.54), creating different tendencies for Al and Ti to attract and donate electrons respectively. This suggests that there are Al-O-Ti bonds and that an alloy not laminate has been formed. The O 1s CLs also indicate the formation of alloyed layers, as shown in Fig. 4(c). The O 1s CL shifts as a function Al:Ti ratio between the two BE extremities of Al_2O_3 (531.16 eV) and TiO_2 (530.0 eV). Furthermore, the FWHM of O 1s CL decreases from binary Al_2O_3 to TiO_2, which again suggests an alloy being formed rather than separate layers of both (laminate), as the FWHM would be larger if the peak contained components from Al_2O_3 and TiO_2 simultaneously (22).

Figures 5 (a)-(b) depict fitting of Al 2p and O 1s CLs for bulk Al_2O_3, while Figs. 5(c)-(d) refer to fitted Ti 2p and O 1s for bulk TiO_2. As seen in Fig. 5(a), the Al 2p is symmetric, suggesting only one environment of Al. The BE of the Al 2p was found at 74.54 eV, in agreement with the reported values (40,41) when different C 1s spectra calibration has been considered. The O 1s peak shown in Fig. 5(b), on the other hand, is fitted with two components, at 531.16 eV associated with Al-O bonds (40) and the other at 531.89 eV

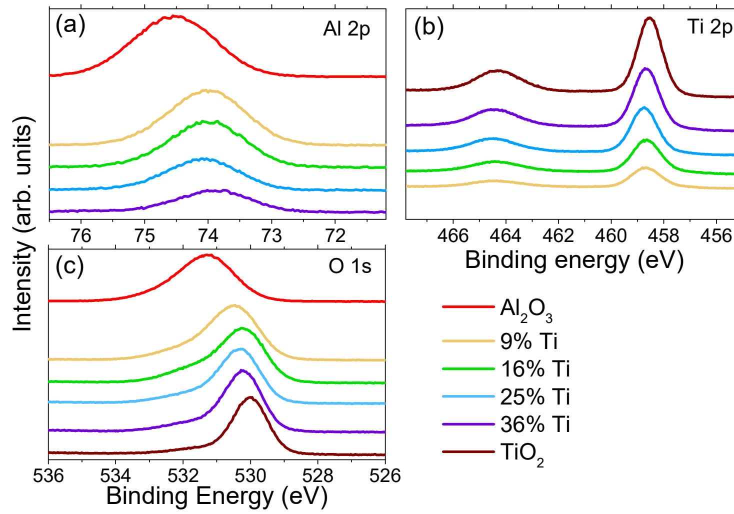

Figure 4. (a) Al 2p, (b) Ti 2p and (c) O 1s XPS CL spectra for bulk (20 nm) ALD AlTiO/GaN stacks with Al_2O_3/GaN and TiO_2/GaN as reference samples.

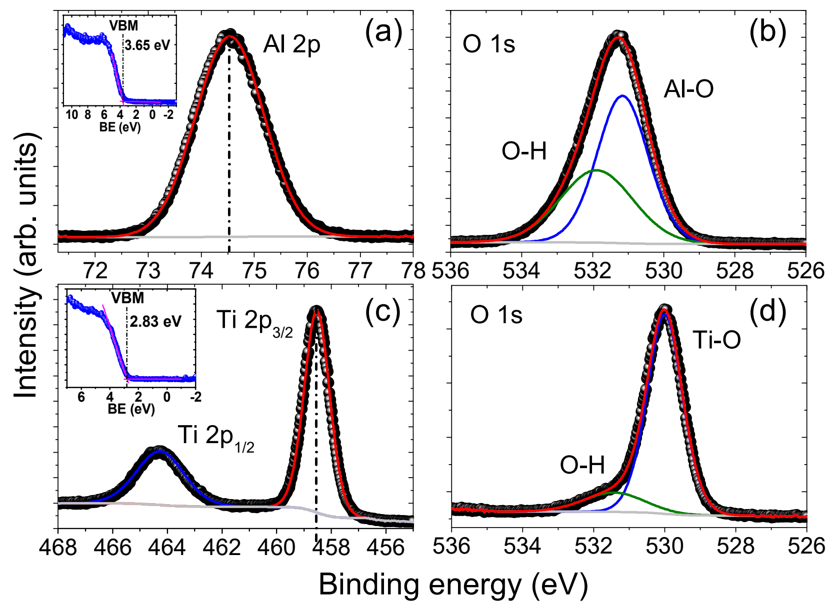

Figure 5. (a)-(b) Al 2p and O 1s fitted CL spectra for bulk Al_2O_3 film; (c)-(d) Ti 2p and O 1s fitted CL spectra for bulk TiO_2 film. The insets in (a) and (c) refer to valence band spectra depicting extraction of valence band maxima for Al_2O_3 and TiO_2 respectively.

likely to be related to O-H species. The latter is not thought to be related to Al-OH bonds since both Al 2p and Al 2s (not shown) CLs are found to be symmetric, indicating only one environment of Al (42,43). The VB spectrum for Al_2O_3 bulk sample is shown in the inset of Fig. 5(a) with VBM at 3.65 eV, which gives the Al 2p CL BE to VBM difference of δ_{Al2O3} = 70.89 eV. The Ti 2p CL shown in Fig. 5(c) is fitted with two components (Ti $2p_{3/2}$ and Ti $2p_{1/2}$), which indicates the presence of only one oxidation state of Ti (+4). The FWHM of the Ti $2p_{1/2}$ is larger than that of the Ti $2p_{3/2}$ due to the Coster-Kronig process (44). Therefore, the area and the BE position of the Ti $2p_{1/2}$ were constrained and the

FWHM was set as a fitting parameter. The O 1s CL had a secondary contribution at the similar BE as the one in Al_2O_3 (Fig. 5(d)), which was attributed to O-H bonds. The latter were not thought to be Ti-OH bonds as the Ti CLs only consisted of Ti-O contribution. Since the VBM of bulk TiO_2 sample was at 2.83 eV (see inset in Fig. 5(c)), the Ti $2p_{3/2}$ to VBM difference was found to be δ_{TiO2} = 455.70 eV. The valence band offset between oxide and GaN can be calculated using XPS and Kraut's method (45) by using the equation:

$$VBO = \delta_{SUB} - \delta_{OXIDE} + \delta_{INT} \quad [2]$$

where δ_{SUB} refers to the binding energy difference of respective CL in the substrate (in our case, Ga $2p_{3/2}$ CL) and VBM for GaN substrate, δ_{OXIDE} of chosen CL in the bulk of the oxide (Al 2p or Ti $2p_{3/2}$) and VBM for bulk oxide sample, and δ_{INT} of Ga $2p_{3/2}$ and Al 2p (or Ti $2p_{3/2}$) from respective oxide and GaN for interfacial oxide/GaN sample. Fig. 6 shows fitted CL spectra and VBM referring to TiAlO oxide with 25% Ti and the three terms in Eq. [2] are calculated to be δ_{SUB} = 1115.24 eV (Fig. 6(a)), δ_{INT} = 1043.60 eV (Fig. 6(b)) and δ_{TiAlO} = 71.0 eV. Note that the Ti 2p peaks sit in the middle of the Ga Augers, hence the Al 2p CL was used in the Kraut's method for all $Ti_xAl_{1-x}O_y$/GaN samples. In case of TiO_2/GaN, the Ti $2p_{3/2}$ was used, but VBO (Eq. [2]) was also cross-checked with Ti 3p CL.

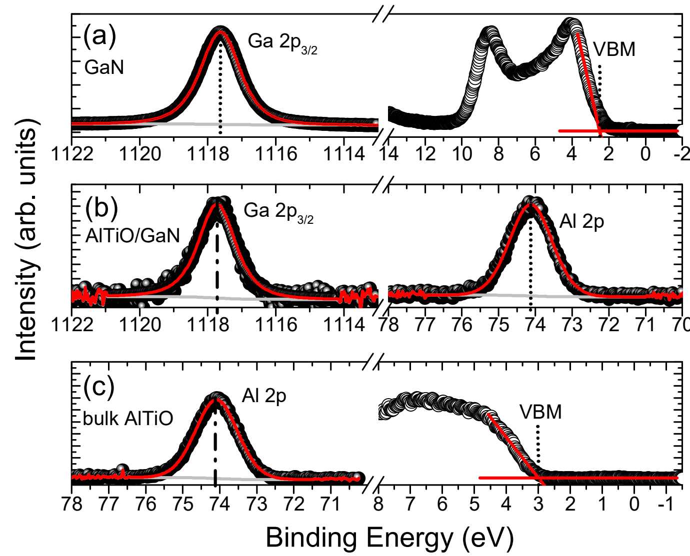

Figure 6. Ga $2p_{3/2}$, Al 2p XPS CLs and VBM extraction from (a) GaN substrate; (b) interfacial 3.9 nm $Ti_xAl_{1-x}O_y$/GaN and (c) bulk 30.9 nm $Ti_xAl_{1-x}O_y$, for x= 25%.

A summary of CL positions, thicknesses, band gaps and band offsets for all $Ti_xAl_{1-x}O_y$/GaN samples is given in Table I. The CBO is calculated from

$$CBO = E_g^{OXIDE} - E_g^{GaN} - VBO \quad [3]$$

where E_g^{OXIDE}, E_g^{GaN} refer to band gaps of oxide (see Table I) and GaN (=3.4 eV (46)) respectively. It is worth mentioning that there is no significant shift of Ga $2p_{3/2}$ for interfacial TiAlO/GaN samples when compared to the BE value of 1117.67 eV for GaN substrate, being indicative of a negligible band bending (BB) at the interface (see Table I). In case of TiO_2/GaN, the Ga $2p_{3/2}$ shifts slightly towards higher BEs, and this could be a

signature of a small downward BB of 0.22 eV. Furthermore, the XPS CL fitting results suggest no interfacial layer is formed between the TiAlO and GaN. The latter is underpinned by (i) the BE positions and FWHM of the O 1s CLs remaining the same (no other oxygen environment), (ii) the Ga 2p FWHM being constant (indicating no new Ga environment) and (iii) symmetry of Ga 2p and Al 2p CLs, for all interfacial mixed oxide samples. Only for interfacial TiO_2/GaN sample, there was an additional component in the Ti 2p CL fitting at 557.33 eV (not shown), which was attributed to Ti_2O_3 in line with the previous XPS studies (47). This interfacial layer and a possible existence of Ga-O bonds at the interface could be a source of positive charges on the GaN surface (48) leading to accumulated surface and resulting in a small downward band bending for this sample.

TABLE I. A summary of fitted binding energies of Al 2p, Ti $2p_{3/2}$, Ga $2p_{3/2}$ XPS CLs and extrapolated VBM for bulk and interfacial $Ti_xAl_{1-x}O_y$/GaN samples fabricated by ALD in this work. The thickness and optical band gap are determined using VASE. The VBO (± 0.25 eV) of deposited oxides on GaN stated is calculated from the Kraut's method (Eq. [2]), while CBO using Eq. [3]. Al_2O_3 and TiO_2 are added as reference samples.

Sample	Thickness (nm)	Al 2p (eV)	Ti $2p_{3/2}$ (eV)	Ga $2p_{3/2}$ (eV)	VBM (eV)	E_g (eV)	VBO (eV)	CBO (eV)
GaN		--	--	1117.67	2.43	3.4*	--	--
Al_2O_3	19.1	74.54	--	--	3.65	6.48	1.13	1.95
	3.0	74.50		1117.72	--			
9% Ti	23.8	74.02	458.66	--	3.13	4.28	0.84	0.04
	3.7	74.23	458.86	1117.74	--			
16% Ti	26.6	74.01	458.64	--	2.97	4.20	0.76	0.04
	3.9	74.14	458.73	1117.58	--			
25% Ti	30.9	74.08	458.74	--	3.08	4.02	0.64	0.02
	3.9	74.12	458.75	1117.72	--			
36% Ti	28.1	73.91	458.66	--	3.01	3.88	0.61	-0.13
	4.0	74.07	458.75	1117.80	--			
TiO_2	17.0	--	458.53	--	2.83	3.65	0.39	-0.14
	3.4		458.74	1117.89	--			

*Ref. 46.

The VBO for Al_2O_3 of 1.13 ± 0.25 eV is in excellent agreement with the recent study (see Ref. 48 and references therein). As can be seen from Table I, the VBO decreases from 0.84 eV for 9% Ti to 0.61 eV for 36% Ti mixed oxide. By inserting optical band gap values from Fig. 3(a) in Eq. [3], the CBO is found to be very small <0.05 eV for mixed oxides with up to 25% Ti. In case of 36% Ti sample and TiO_2/GaN, type I heterojunction is observed with CBO of around -0.1 eV. TiO_2 was found to have VBO of 0.39 ± 0.25 eV. In the previous XPS study of TiO_2/GaN, Ga 3d and Ti 3p CLs were used in the Kraut's method where VBO = -0.09 ± 0.25 eV has been obtained (13); both Ga 3d and Ti 3p are shallow CLs and have a tendency to hybridize with s-levels at the bottom of the valence band amounting to reducing accuracy in VBO estimation. Therefore, in this work we have used Ga $2p_{3/2}$ and Ti $2p_{3/2}$ CLs. Furthermore, the δ_{SUB} for GaN has been measured to be 17.05 eV (13), being much smaller than widely cited literature values of 17.7-17.8 eV (48); if the latter value for δ_{SUB} is used in the Kraut's method, the VBO is 0.55 ± 0.25 eV (13) in line with the measured value in this work within the accuracy of the method. It has also been reported recently that VBO for TiO_2/AlGaN is 0.56 eV and for Al_2O_3/AlGaN is 1.00 eV by XPS and Kraut's method (14); from these values the VBO of 1.56 eV for TiO_2/Al_2O_3 interface can be deduced in excellent agreement with 1.52 eV from this study calculated from measured VBOs for TiO_2/GaN (0.39 eV) and Al_2O_3/GaN (1.13 eV) (see Table I). It is worth mentioning that due to a smaller band gap of 3.0 eV for TiO_2 used for the band alignment in Ref. 13, the type II TiO_2/GaN heterojunction has been deduced. In this study,

the measured optical band gap by VASE has been found to be larger (3.65 eV, Fig. 3(a), Table I) and hence gives type I heterointerface. Note that the difference in valence band maxima for the bulk oxide samples and GaN are in close agreement with the VBOs calculated from Kraut's method and Eq. [2], providing further evidence of negligible band bending at oxide/GaN interfaces for samples listed in Table I.

Electrical properties of $Ti_xAl_{1-x}O_y$ films on GaN

CV and IV measurements of MIS capacitors based on $Ti_xAl_{1-x}O_y$ alloy films, with the compositional range of 9–36% Ti, were carried out for the thickness range from 24 nm to 31 nm (Table I). The current density (J) vs. gate voltage plots are shown in Fig. 7(a), clearly indicating a rise of gate leakage when Ti% is increased in the mixed oxide films. Fig. 7(b) shows J at 1 MV/cm from the $Ti_xAl_{1-x}O_y$ compositional range in this work and Ref. 22. The Ti-rich film (36% Ti) has J = 2.98×10^{-1} A/cm^2 decreasing to 3.95×10^{-5} A/cm^2 for Al-rich film (9% Ti), being comparable to the previously reported values of RTA annealed (700ºC for 60 seconds in N_2) ALD deposited $Ti_xAl_{1-x}O_y$ films (22). The permittivity of the oxide films was extracted from the CV plots at 1 MHz; the results are depicted in Fig. 7(b) and show increase of k from 7.0 (Al_2O_3), 10.2 (9% Ti), 15.6 (16% Ti), 24.4 (25% Ti), 32.9 (36% Ti) to 75.8 (TiO_2) with increasing Ti content in the mixed oxides. The k values obtained for Al_2O_3 and TiO_2 are in line with the range reported in the literature (15,19).

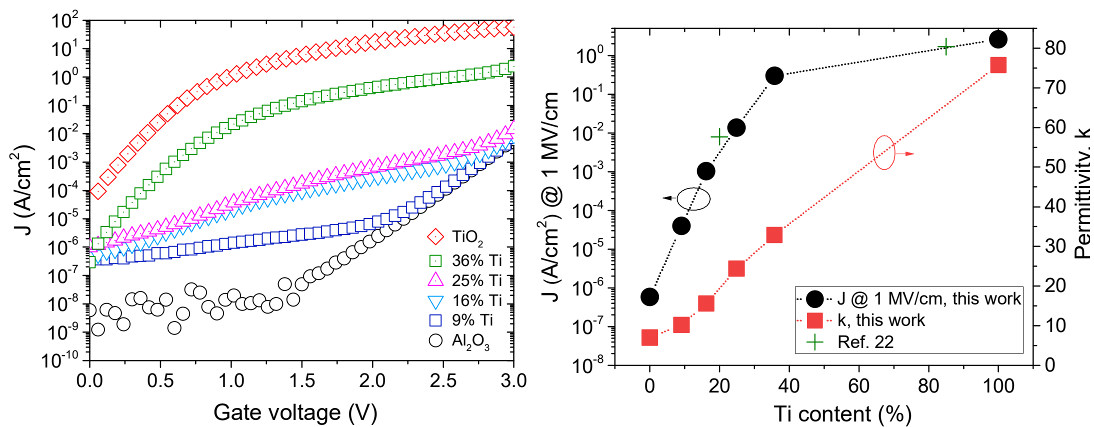

Figure 7. (a) Current density (J) vs. gate voltage; (b) J at 1 MV/cm and k vs % Ti measured from MIS capacitors based on ALD $Ti_xAl_{1-x}O_y$ films. (Device area A = 4.9×10^{-8} m^2.)

ALD $Ga_xAl_{1-x}O_y$ films on GaN

Band alignment of Ga_2O_3 on GaN

Figure 8(a) depicts the Ga $2p_{3/2}$ XPS CL spectra for the bulk GaN (top), interfacial Ga_2O_3/GaN (middle) and bulk Ga_2O_3 (bottom) samples. The Kraut's method (45) and Eq. [2] was used to find the VBO between Ga_2O_3 and GaN. It can be seen for the interfacial Ga_2O_3/GaN sample that the Ga $2p_{3/2}$ peak is resolved into two components at low BE side at (i) 1117.74 eV related to Ga-N bond, and (ii) at high BE side at 1118.26 eV referring to Ga-O bond. This is due to the electronegativity of oxygen being greater than that of nitrogen leading to the Ga CL from Ga_2O_3 to be found at higher BE. Hence, the respective

δ_{INT} = 0.52 eV. For GaN substrate and bulk Ga_2O_3 (of 22.2 nm thickness as measured by VASE), the position of the Ga $2p_{3/2}$ peak was found at 1117.22 eV (Fig. 8(a), top) and 1118.30 eV (Fig. 8(a), bottom) respectively. The valence band maximum was found by extrapolating the valence band edge and finding the point of intersection between this linear fit and the background linear fit (Fig. 8(b)). For GaN and Ga_2O_3 the VBMs (± 0.25 eV) were found to be 2.07 eV and 3.36 eV, respectively. These values were used to calculate δ_{SUB} = 1115.15 eV and δ_{Ga2O3} = 1114.94 eV. The VBO for Ga_2O_3/GaN is then calculated from Eq. [2] and found to be 0.73 ±0.25 eV. The IPES spectra were used to find the conduction band minima (CBM, ± 0.25 eV) for GaN (1.60 eV) and Ga_2O_3 (1.23 eV) as shown in the left hand side of Fig. 8(b). Since both the VBM and CBM are measured with respect to the Fermi level, the addition of the two values gives the band gap of the material. Therefore, the band gap (± 0.25 eV) measured by XPS/IPES is found to be 3.67 eV for GaN and 4.59 eV for Ga_2O_3.

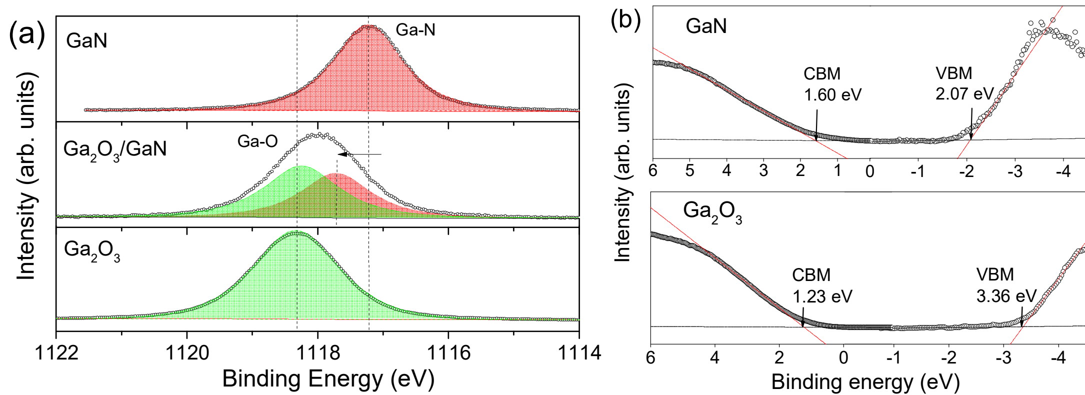

Figure 8. (a) Ga $2p_{3/2}$ XPS CL fitting for GaN (top), interfacial Ga_2O_3/GaN (middle) and bulk Ga_2O_3 (bottom) ALD film; (b) IPES spectra for GaN (top) and Ga_2O_3 (bottom).

There is an indication of substantial downward band bending of 0.52 eV from the shift of Ga $2p_{3/2}$ in GaN substrate and in Ga_2O_3/GaN (see dashed lines and an arrow in Fig. 8(a)). The angle resolved (AR)-XPS data confirm ~0.5 eV shift of Ga $2p_{3/2}$ peak towards the higher BEs with decrease of take-off angle (TOA) from normal to the surface (90°, BE = 1117.78 eV) to 15° from the surface (BE = 1118.28 eV), providing further evidence of substantial downward band bending at Ga_2O_3/GaN interface. The downward BB of GaN surface has been reported following similar ex-situ chemical cleaning as in this work (49). The observation of an accumulated GaN surface has been explained by a significant positive charge density residing within the native oxide (49,50). A possible source for the positive charge may be (i) interfacial fixed charge with energy states between the CBM of the native oxide and GaN (50); or (ii) a possible polarity inversion of the GaN surface, that is a change in the spontaneous polarization charge from negative to positive due to the formation of Ga–O bonds.

The band gap of GaN from Fig. 8(b) (top) is higher (3.67 eV) than the reported optical band gap of 3.4 eV (46), but it is within the experimental error (± 0.25 eV) of the IPES measurements. The optical band gap of Ga_2O_3 extracted from the VASE B-spline model and associated absorption coefficient vs. photon energy curve shown in Fig. 9(a) is 4.47 ± 0.1 eV and compares to 4.59 ± 0.25 eV derived from the XPS/IPES (Fig. 8(b), bottom). The obtained values are in agreement with the literature (23,24).

Band alignment and electrical properties of $Ga_xAl_{1-x}O_y$ on GaN

A set of 20 nm (nominal) $Ga_xAl_{1-x}O_y$ on GaN samples was fabricated varying the Ga:Al ALD cycles from 1:19, 1:4, 4:1 and 19:1, referring to x of 5% Ga, 20% Ga, 80% Ga and 95% Ga respectively. Since MIS capacitor devices exhibited very high leakage current for samples with high Ga content and no measurable CV plots, the focus was on investigating only films with high Al content. The O 1s XPS ELS spectra in Fig. 9(b) for samples with high Al doping show significant increase in the band gap (± 0.25 eV) from 5.50 eV (80% Al) to 5.98 eV (95% Al).

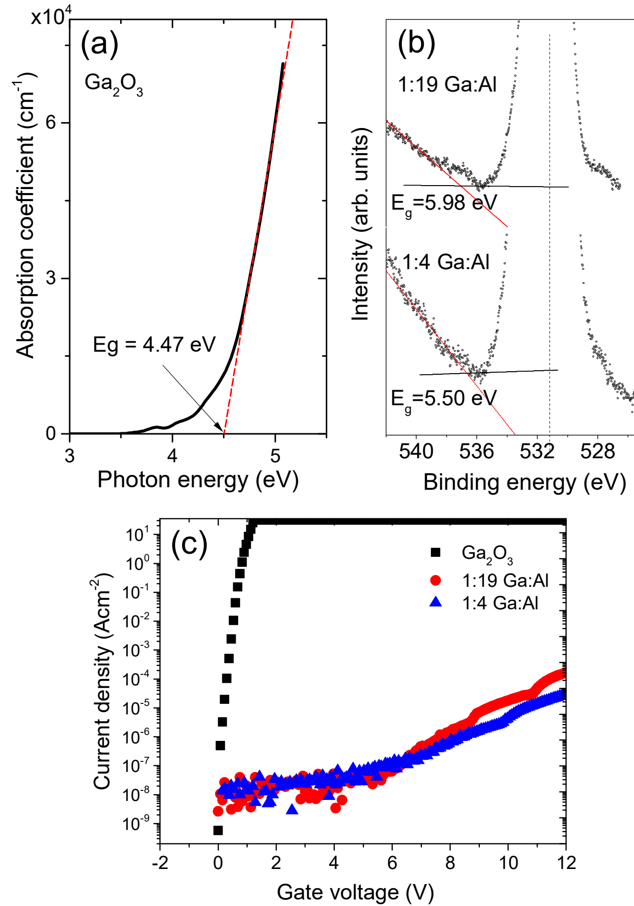

Figure 9. α vs. E for Ga_2O_3; (b) O 1s ELS spectra for 5% Ga (95% Al, 1:19=Ga:Al) and 20% Ga (80% Al, 1:4=Ga:Al); (c) Current density vs. voltage for associated MIS capacitors.

The valence band maxima extracted from the linear extrapolation of the VB edge (spectra not shown) give values of 3.29 eV for 5% Al doped sample and a constant value of 3.6 ± 0.2 eV for 20%, 80% and 95% Al doped samples. Given the VBM = 2.07 eV for GaN (Fig. 8(b)), the results suggest no change in VBO when Al content is increased from 20% to 95%, i.e. VBO is ~1.5 eV. Note that using the VBM values for Ga_2O_3 and GaN, the VBO for Ga_2O_3/GaN is estimated to be 1.36 eV, a larger value than the one measured from the Kraut's method (0.73 eV). However, by taking into account the observed downward BB of 0.52 eV, the VBO further from the interface can be deduced to be 1.25 ± 0.25 eV close to the estimated value of 1.36 eV. The latter is in agreement with the VBO

of 1.4 ± 0.08 eV reported for β−Ga_2O_3/GaN heterostructure derived from XPS CLs Ga 3d, N 1s and O 1s, and by Kraut's method where no BB has been observed at the interface (26).

The CBO is calculated using Eq. [3] taking into account the optical band gap for Ga_2O_3 and gives a small value of 0.34 ± 0.25 eV. The latter explains very high leakage currents observed for MIS capacitors based on Ga_2O_3 and low Al-doped Ga_2O_3 films. For high Al doping (80% and 95%), the band gap increases significantly and since the VBO is observed not to change, the CBO is found to increase to 0.6 eV (for 80% Al) and to 1.1 eV (for 95% Al). Fig. 9 (c) shows significant reduction of leakage current of several orders of magnitude for high Al-doped samples in agreement with the band line-up study. The permittivity of $Ga_xAl_{1-x}O_y$ films is found to be ~ 7 from CV plots close to the value of k for Al_2O_3 film (Fig. 7(b)) as these films are highly doped with Al.

In summary, the band alignments of $Ti_xAl_{1-x}O_y$/GaN and $Ga_xAl_{1-x}O_y$/GaN stacks studied in this work are presented schematically in Fig. 10.

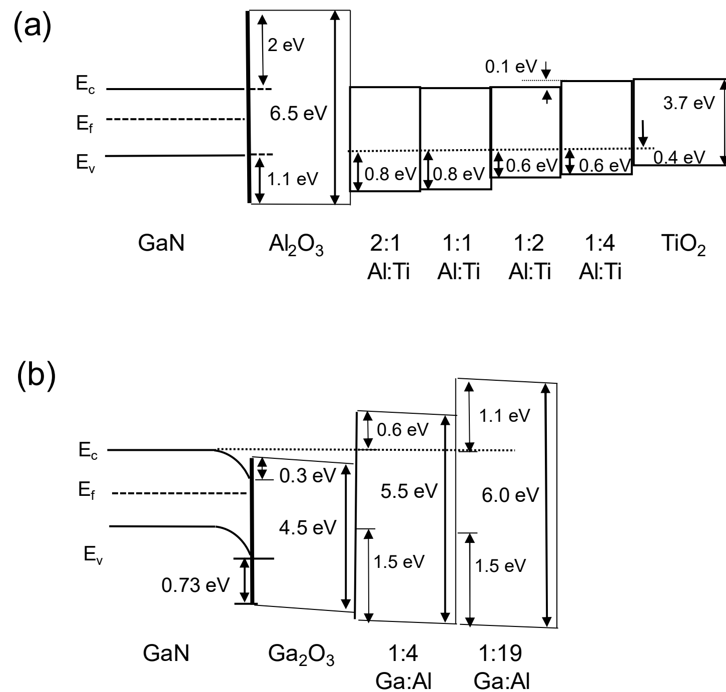

Figure 10. The experimentally derived band line-up for ALD processed (a) $Ti_xAl_{1-x}O_y$/GaN and (b) $Ga_xAl_{1-x}O_y$/GaN stacks. (The diagrams are not to scale.)

Summary

In this paper, $Ti_xAl_{1-x}O_y$ (x = 9% to 100%) and $Ga_xAl_{1-x}O_y$ (x= 5%, 20%, 80% and 95%) films have been fabricated using atomic layer deposition with the aim of achieving favorable band alignment with GaN for MIS-HEMT applications. X-ray photoelectron spectroscopy, inverse photoemission spectroscopy and variable angle spectroscopic ellipsometry were used to estimate the band alignment and interfacial properties. Although

the permittivity of $Ti_xAl_{1-x}O_y$ increases significantly from 7 for Al_2O_3 to 24.4 for 25% Ti and 32.9 for 36% Ti, the band line-up of these mixed oxides is not ideal as conduction band offsets with GaN were found to be < 0.1 eV. The VBO is found to decrease from 0.8 eV for 9% Ti to 0.6 eV for 36% Ti mixed oxide film. The TiO_2/GaN was found to be type I heterojunction interface with VBO = 0.39 ± 0.25 eV. The results from Ga_2O_3 and $Ga_xAl_{1-x}O_y$ films point to substantial increase of the band gap from ~4.6 eV for Ga_2O_3 to 5.9 eV for the 1:19 Ga:Al ALD cycles (5% Ga) doped sample and a strong suppression of leakage current. The VBO for Ga_2O_3/GaN interface is found to be 0.73 ± 0.25 eV with a substantial downward band bending observed at the GaN surface. The VBM for $Ga_xAl_{1-x}O_y$ with x=5% and 20% remains constant, indicating an increase in CBO in line with improved gate leakage current. The results are promising for future applications in GaN based devices.

Acknowledgments

The authors acknowledge UGC-UKIERI project numbers IND/CONT/G/17-18/18 and F.No.184-1/2018(IC) “Dielectric engineering on GaN for sustainable energy applications” funded by the British Council; UKRI GCRF GIAA award 2018/19 and “Digital in India” project no. EP/P510981/1 funded by the EPSRC, UK.

References

1. H. Amano, Y. Baines, E. Beam, M. Borga, T. Bouchet, P. R. Chalker, M. Charles, K. J. Chen, N. Chowdhury, R. Chu, C. D. Santi, M. M.D. Souza, S. Decoutere, L. D. Cioccio, B. Eckardt, T. Egawa , P. Fay , J. J. Freedsman, L. Guido, O. Häberlen, G. Haynes, T. Heckel, D. Hemakumara, P. Houston, J. Hu, M. Hua, Q. Huang, A. Huang, S. Jiang, H. Kawai, D. Kinzer, M. Kuball, A. Kumar, K. B. Lee, X. Li, D. Marcon, M. März, R. McCarthy, G. Meneghesso, M. Meneghini, E. Morvan, A. Nakajima, E. M. S. Narayanan, S. Oliver, T. Palacios, D. Piedra, M. Plissonnier, R. Reddy, M. Sun, I. Thayne, A. Torres, N. Trivellin, V. Unni, M. J. Uren, M. V. Hove, D. J. Wallis, J. Wang, J. Xie, S. Yagi, S. Yang, C. Youtsey, R. Yu, E. Zanoni, S. Zeltner, and Y. Zhang, *J. Phys. D. Appl. Phys.* **51**, 163001 (2018).
2. K.J. Chen, O. Häberlen, A. Lidow, C. L. Tsai, T. Ueda, Y. Uemoto, and Y. Wu, *IEEE Trans. Electron Devices* **64**, 779 (2017).
3. T. Hashizume, S. Ootomo, and H. Hasegawa, *Appl. Phys. Lett*. **83**, 2952 (2003).
4. C. Liu, E. F. Chor, and L. S. Tan, *Appl. Phys. Lett.* **88**, 173504 (2006).
5. D. Ye, B. Yang, K. K. Ng, J. Bude, G. D. Wilk, S. Halder, and J. C. M. Hwang, *Appl. Phys. Lett*. **86**, 063501 (2005).
6. P. Kordoš, G. Heidelberger, J. Bernát, A. Fox, M. Marso, and H. Lüth, *Appl. Phys. Lett.* **87**, 143501 (2005).
7. S. Arulkumaran, T. Egawa, H. Ishikawa, T. Jimbo, and Y. Sano, *Appl. Phys. Lett*. **84**, 613 (2004).
8. F. Tian and E. F. Chor, *J. Electrochem. Soc*. **157**, H557 (2010).
9. H. Jiang, C. Liu, K. W. Ng, C.W. Tang, and K. M. Lau, *IEEE Trans. Electron Devices* **65**, 5337 (2018).
10. T.J. Anderson, V. D. Wheeler, D. I. Shahin, M. J. Tadjer, A. D. Koehler, K. D. Hobart, A. Christou, F. J. Kub, and C. R. Eddy, *Appl. Phys. Express* **9**, 071003 (2016).
11. D. A. Deen, D. F. Storm, R. Bass, D. J. Meyer, D. S. Katzer, S. C. Binari, J. W. Lacis, and T. Gougousi, *Appl. Phys. Lett*. **98**, 023506 (2011).

12. S. Yang, S. Huang, M. Schnee, Q. T. Zhao, J. Schubert, and K. J. Chen, *IEEE Trans. Electron Devices* **60**, 3040 (2013).
13. P. J. Hansen, V. Vaithyanathan, Y. Wu, T. Mates, S. Heikman, U. K. Mishra, R. A. York, D. G. Schlom, and J. S. Specka, *J. Vac. Sci. Technol. B* **23**, 499 (2005).
14. A. Rawat, M. Meer, V. kumar Surana, N. Bhardwaj, V. Pendem, N. S. Garigapati, Y. Yadav, S. Ganguly, and D. Saha, *IEEE Trans. Electron Devices* **65**, 3725 (2018).
15. T. Fuyuki and H. Matsunami, *Jpn. J. Appl. Phys*. **25**, 1288 (1986).
16. J. Yan, D. C. Gilmer, S. A. Campbell, W. L. Gladfelter, and P. G. Schmid, *J. Vac. Sci. Technol. B* **14**, 1706 (1996).
17. J. Aarik, A. Aidla, A.-A. Kiisler, T. Uustare, and V. Sammelselg, *Thin Solid Films* **305**, 270 (1997).
18. Q. Xie, J. Musschoot, D. Deduytsche, R. L. V. Meirhaeghe, C. Detavernier, S. V. D. Berghe, Y. L. Jiang, G. P. Ru, B. Z. Li, and X. P. Qu, *J. Electrochem. Soc*. **155**, H688 (2008).
19. X. Qin, L. Cheng, S. McDonnell, A. Azcatl, H. Zhu, J. Kim, and R.M. Wallace, *J. Mater. Sci: Mat. in El.* **26**, 4638 (2015).
20. B.M. Reddy, B. Chowdhury, and P.G. Smirniotis, *Appl. Cat. A: General* **211**, 19 (2001).
21. L.H. Kim, K. Kim, S. Park, Y.J. Jeong, H. Kim, D.S. Chung, S.H. Kim, and C.E. Park, *ACS Appl. Mat. & Inter*. **6**, 6731 (2014).
22. A. P. Alekhin, A. A. Chouprik, S. A. Gudkova, A. M. Markeev, Y. Y. Lebedinskii, Y. A. Matveyev, and A. V. Zenkevich, *J. Vac. Sci. Techn. B* **29**, 01A302 (2011).
23. H-Y. Shih, F-C. Chu, A. Das, C-Y. Lee, M-J. Chen, and R-M. Lin, *Nanoscale Research Letters* **11**, 235 (2016).
24. D-W. Choi, W-B. Chung, and J-S. Park, *Thin Solid Films* **546**, 31 (2013).
25. H.S. Oon and K.Y. Cheong, *Mat. Sci. Semicond. Proc*. **16**, 1217 (2013).
26. W. Wei , Z. Qin, S. Fan, Z. Li, K. Shi, Q. Zhu, and G. Zhang, *Nanoscale Research Letters* **7**, 562 (2012).
27. S.D. Wolter, J.M. DeLucca, S.E. Mohney, R.S. Kern, and C.P. Kuo, *Thin Solid Films* **371**, 153 (2000).
28. P. Lagger, C. Ostermaier, G. Pobegen, and D. Pogany. Proc. IEEE IEDM, p. 299 (2012).
29. S. Huang, S. Yang, J. Roberts, and K.J. Chen, *Jpn. J. Appl. Phys*. **50**, 110202 (2011).
30. D.A. Shirley, *Phys. Rev. B* **5**, 4709 (1972).
31. S.A. Chambers, T. Droubay, T. C. Kaspar, and M. Gutowski, *J. Vac. Sci. Technol. B* **22**, 2205 (2004).
32. Z. Wang, R. Zhang, H. Lu, X. Chen, Y. Sun, Y. Zhang, Y. Wei, J. Xu, S. Wang, Y. Zheng, and L. Chen, *Nanoscale Res. Lett.* **10**:46, 1 (2015).
33. M. Horprathum, P. Chindaudom, P. Limnonthakul, P. Eiamchai, N. Nuntawong, V. Patthanasettakul, A. Pokaipisit, and P. Limsuwan, *J. Appl. Phys*. **108**, 013522 (2010).
34. N.Y. Garces, D.J. Meyer, V.D. Wheeler, Z. Liliental-Weber, D.K. Gaskill, and C.R. Eddy Jr., *J. Vac. Sci. Techn. B* **32**, 03D101 (2014).
35. Y. Shi, R. Zhang, H. Zheng, D. Li, W. Wei, X. Chen, Y. Sun, Y. Wei, H. Lu, N. Dai, and L. Chen, *Nanoscale Res. Lett.* **12**, 1 (2017).
36. M. T. Nichols, W. Li, D. Pei, G. A. Antonelli, Q. Lin, S. Banna, Y. Nishi, and J. L. Shohet, *J. Appl. Phys.* **115**, 094105 (2014).
37. I.Z. Mitrovic, M. Althobaiti, A.D. Weerakkody, V.R. Dhanak, N. Sedghi, S. Hall, P.R. Chalker, D. Tsoutsou, and A. Dimoulas, *J. Appl. Phys*. **115**, 114102 (2014).

38. B. M. Reddy, B. Chowdhury, and P. G. Smirniotis, *Appl. Catalysis A: General* **211**, 19 (2001).
39. L. H. Kim, K. Kim, S. Park, Y. J. Jeong, H. Kim, D. S. Chung, S. H. Kim, and C. E. Park, *ACS Appl. Mater. Interfaces* **6**, 6731 (2014).
40. T. Gougousi, D. Barua, E.D. Young, and G.N. Parsons, *Chem. Mater*. **17**, 5093 (2005).
41. B. Lee, S. Park, H. Kim, K. Cho, E. M. Vogel, M. J. Kim, R. M. Wallace, and J. Kim, *Appl. Phys. Lett*. **92**, 203102 (2008).
42. I. Iatsunskyi, M. Kempinski, M. Jancelewicz, K. Zaleski, S. Jurga, and V. Smyntyna, *Vacuum* **113**, 52 (2015).
43. J. Haeberle, K. Henkel, H. Gargouri, F. Naumann, B. Gruska, M. Arens, M. Tallarida, and D. Schmeißer, *J. Nanotechnol.* **4**, 732 (2013).
44. D. Coster and R.D.L. Kronig, *Physica* **48**, 13 (1928).
45. E. A. Kraut, R. W. Grant, J. R. Waldrop, and S. P. Eowalczyk, *Phys. Rev. Lett*. **44**, 1620 (1980).
46. J. Wagner, H. Obloh, M. Kunzer, M. Maier, K. Köhler, and B. Johs, *J. Appl. Phys*. **89**, 2779 (2001).
47. M. J. Jackman, A. G. Thomas, and C. Muryn, *J. Phys. Chem. C* **119**, 13682 (2015).
48. S.N. Supardan, P. Das, J.D. Major, A. Hannah, Z.H. Zaidi, R. Mahapatra, K. B. Lee, R. Valizadeh, P.A. Houston, S. Hall, V.R. Dhanak, and I.Z. Mitrovic, *J. Phys. D: Appl. Phys.* **53**, 075303 (2020).
49. T.L. Duan, J.S. Pan, and D.S. Ang, *ECS J. Solid State Sci. Technol.* **5** P514 (2016).
50. M. Esposto, S. Krishnamoorthy, D.N. Nath, S. Bajaj, T.H. Hung, and S. Rajan, *Appl. Phys. Lett.* **99**, 133503 (2011).